# Inside the flux footprint: Understanding the role of

# organized land cover heterogeneity on land-atmosphere

# exchange fluxes

- Leila C Hernandez Rodriguez <sup>1</sup>, Allison E Goodwell <sup>3</sup>, Praveen Kumar <sup>1,2</sup>
- <sup>1</sup>Department of Civil and Environmental Engineering, University of Illinois at Urbana-Champaign,
- 6 Champaign, Illinois, USA
- <sup>2</sup>Department of Atmospheric Sciences, University of Illinois at Urbana-Champaign, Champaign, Illinois,
  - USA
- <sup>3</sup>Department of Civil Engineering, University of Colorado Denver, Denver, Colorado, USA

Corresponding author: P. Kumar, kumar1@illinois.edu

#### Abstract

10

11

12

13

14

15

16

17

20

21

22

23

24

25

27

32

Eddy covariance measurements quantify the magnitude and temporal variability of landatmosphere exchanges of water, heat, and carbon dioxide  $(CO_2)$  among others. However, they also carry information regarding the influence of spatial heterogeneity within the flux footprint, the temporally dynamic source/sink area that contributes to the measured fluxes. A 25m tall eddy covariance flux tower in Central Illinois, USA, a region where drastic seasonal land cover changes from intensive agriculture of maize and soybean occur, provides a unique setting to explore how the organized heterogeneity of row crop agriculture contribute to the estimates of land-atmosphere exchange from the observations. We characterize the effects of this heterogeneity on latent heat (LE), sensible heat (H), and  $CO_2$  fluxes  $(F_c)$  using a combined flux footprint and ecohydrological modeling approach. For three years from 2016 to 2019, we estimate the relative contribution of each crop type resulting from the structured spatial organization of the land cover to the observed fluxes. Since the wind direction, magnitude and stability varies at each time step, the net contribution of each crop to the overall observed flux is a result of both the relative abundance of a crop and the magnitude of its flux contribution in the dynamically changing flux footprint. The combined action of hydroclimatological drivers and the organized heterogeneity of the land cover explains the inter-annual variations of flux exchange. This study helps us understand how the observed flux magnitudes and variability depend on the organized land cover heterogeneity and is extensible to other intensively managed or otherwise heterogeneous landscapes.

# **Key Words:**

- Land cover heterogeneity
- Eddy covariance
- Flux footprint
  - Ecohydrological modeling
- Critical Zone Science
- Intensively Managed Landscapes

# Plain Language Summary

Maize (corn) and soybean fields throughout the agricultural Midwest of the US create a "patchwork quilt" of land cover types. This pattern impacts the exchange of water, heat, and  $CO_2$  flux between the land and atmosphere. Here, we determine the relative contribution of different land cover types to the total flux as measured by a tall eddy covariance flux tower. We estimate the spatial extent contributing to every flux measurement. We combine it with an ecohydrological model to obtain the temporally varying ratio of fluxes for different land covers. Then we estimate how they contribute to the overall flux, which depends on how the crop fields are spatially distributed. We find that the tower mostly "sees" fields located between 168m and 268m away although areas as far away as several kilometers contribute to the observations. Maize fields contributed more than soybean fields during the 2016 and 2018 growing seasons, and vice versa during 2017. We compare our results against a hypothetical case where all vegetation is randomly distributed on the surface. We find that the knowledge of footprint contributions combined with model results helps explain why the observed fluxes vary from year to year.

# 1 Introduction

Agricultural landscapes dominate the US Midwest, influencing ecohydrological responses where the root-soil-canopy-atmosphere continuum act as an integrated system. In this region, small-grain production was replaced about a century ago by maize and soybean row crop agriculture. Today, a seasonal human-induced reorganization of vegetation to meet agricultural ecosystem services determines the spatial distribution (Richardson & Kumar, 2017), and the region experiences seasonal transitions in land cover every year. Specifically, row crop agriculture consists of seed planting in early spring, rapid growth in early summer, maturity in late summer, and harvest during autumn. During July, the US corn belt is now 40% more productive than the Amazonian rain-forest (Foufoula-Georgiou et al., 2015) as a result of steady agricultural intensification over the past two centuries. This dense vegetated land cover during the growing season contrasts drastically with an almost bare landscape of soil, roots, and litter left after harvest typically around mid-October to November (NASS, 2010). During the growing season, a patchy mosaic of different crops is the dominant landscape feature, which partially hides other sources of heterogeneity such as soil properties and micro-topographic variability (Le & Kumar, 2014). In this study, we

70

71

72

73

74

75

77

78

79

80

81

82

83

85

87

90

91

92

93

99

100

focus on the contribution of the "organized land cover heterogeneity", which we define as the human-induced spatial organization of the landscape, on the fluxes exchanged between the landscape and the atmosphere when measured at a tall eddy covariance tower. For example, to measure the dynamic land-atmosphere exchange of heat, water, and carbon dioxide  $(CO_2)$  fluxes in intensively managed agricultural landscapes, such as that located in Illinois, where maize and soybean plots dominate the landscape, a 25m-tall flux tower sees hundreds of agricultural plots inside the dynamic flux footprint at each time step of the measurements (Kirby et al., 2008). We quantitatively address one of the major challenges facing the interpretation of eddy covariance measurements in heterogeneous landscapes: Besides other sources of landscape heterogeneity, how does the human-induced "organized land cover heterogeneity" contribute to the observed fluxes by a tall eddy covariance flux tower?

Eddy covariance measurements require a homogeneous flow field to provide an accurate integration of fluxes at the land-atmosphere interface (Aubinet et al., 2012; Burba, 2013). However, for tall towers the dynamic upwind surface area where the land-atmosphere exchange flux is generated, known as the flux footprint, generally exhibits spatial heterogeneities and fluxes from different sources mix at the observation point (Leclerc & Foken, 2014). The use of footprint models for interpreting micrometeorological observations is a common practice, but the process of differential weighting within a temporally varying flux footprint is a "well-known but frequently overlooked feature of eddy covariance measurements" (Tuovinen et al., 2019; Chu et al., 2021). Previous studies have related eddy covariance flux tower observations to individual land use, mostly using a combination of different measurement techniques at different scales. One approach relies on in situ data, from nearby towers at which flux footprints cover a specific vegetation type (Chi et al., 2020, 2019; Biermann et al., 2014) or from flux chamber measurements (Tuovinen et al., 2019). However, in highly heterogeneous systems with mixed vegetation and soil wetness, it is known that there is a possibility for serious mismatch between eddy covariance flux measurements and in situ measurements for determining specific fluxes associated with a land cover classes. In our case, when tens of plots are located inside the several square kilometers size dynamic flux footprint, on-site measurements might not be representative of the average behavior of each land cover type inside the tower flux footprint, which can potentially bias the conclusions of a study. Another approach relies on the use of remote sensing or aircraft data to estimate fluxes from plots on the flight transect (Kirby et al., 2008). However, the scale of heterogeneity discernible depends on the flight altitude, and if

102

103

104

105

106

107

108

110

111

112

113

114

115

116

117

118

119

121

122

123

124

125

126

127

128

129

130

131

132

133

fluctuations occur during the acquisition of the data, the estimation of fluxes from different sources can be affected. Typically, the use of in situ techniques, such as flux chambers, and remote sensing including aircraft data, are limited to study cases due to their inability to provide continuous observations. To answer our research question, we require to pair the ecosystem scale observations from our tall flux tower, with a technique that can provide continuous data of the average behavior of each land cover type inside its flux footprint. Together, we can determine the relative contribution of each land cover type at every time step of the measurements. Therefore, instead of using scattered observations as representative of the behavior of each land cover type, we estimate the average behavior of each land cover type using an ecohydrological modeling approach. An advantage of pairing the tower observations with modeling results for each land cover type, is the possibility of generalizing the implementation to other land cover types in future studies. Other studies have focused on extracting the time series associated with a plot-nearby to a flux tower. In that case, the time series for the plot is obtained by extracting the fluxes observed by the tower when the plot intermittently lies within the dynamically changing flux footprint. For that purpose, TOVI software (Licor, 2021) can be useful, especially if the plot is located in the upwind direction from the tower. However, many times it requires additional sources of information such as nearby towers or flux chambers, to later recreate a full time series for a plot. Previous studies have used a set of towers with overlapping flux footprints or modeling results for the times when the towers do not see the area of interest (Biermann et al., 2014).

Our work is distinct from these previous efforts, in that we combine observation and ecohydrologic modeling to disentangle the contributions of different crop types to the observed fluxes where the organized heterogeneity plays a direct role in their relative contributions. In particular, it is distinct from and provides further refinement to the approach by Chu et al. (2021) in that we consider a structured heterogeneity in the flux footprint whose contributions are dynamically changing at every measurement time step (15 min). Therefore, it goes beyond the monthly flux footprint climatologies for many Ameriflux sites used by Chu et al. (2021). However, when aggregating over time, the flux footprint climatology blends the sources and sinks of the flux while identifying the spatial extent and temporal dynamics of the areas contributing to the observed fluxes at a tower site. We adopt a more detailed perspective to analyze the relative contribution of each land cover type inside the dynamic flux footprint at each time step (15 min) that results in clear identifications of the contribution to the observation from each crop type as a result of the structure heterogeneity.

The distinctive contribution of this study is to investigate how the combined action of (1) hydroclimatological drivers acting on the ecosystem, and (2) the difference in the fraction of land cover types in the flux footprint due to the organized heterogeneity of the land cover, creates the flux signal observed at the tower. Here we emphasize the role of each land cover type on the measured exchange of water, heat, and  $CO_2$  fluxes at the land-atmosphere interface, which is a critical aspect when accounting for fluxes' sources and sinks from agricultural landscapes (Masson-Delmotte et al., 2021). Given that the change in flux observed at the tower could either correlate to a change in fluxes from the crops or a shift in relative land cover contributions, we analyze the effect of the relative contribution due to maize and soybean within the footprint as a result of wind speed and direction, and atmospheric stability. Using the observations at the tall eddy covariance flux tower and other available data sources in a complementary way, such as flux footprint and ecohydrological modeling results, we are able to provide a more informed interpretation for the behavior of the observed fluxes by a tall tower with respect to the origin of the fluxes in the landscape.

This paper is organized as follows: In Section 2, we describe the Intensively Managed Landscape Critical Zone Observatory (IMLCZO) study site (Wilson et al., 2018), and in Section 3, we present the methods to account for organized land cover spatial heterogeneity, including the considerations for the estimation of the two-dimensional flux footprint and the description of the use of the ecohydrological model to estimate the fluxes of the upwind area sources. Results and discussion are presented in Section 4, where we describe the ecosystem behavior at the study site as observed by the flux tower. Then we explain the results of the flux footprint and the ecohydrological modeling, and we analyze the seasonal and interannual evolution of the flux contribution due to each crop type. At the end of Section 4, we connect maize and soybean crop yield at the study site to investigate  $CO_2$  flux dynamics. In Section 5 we summarize the main findings and discuss some assumptions used in this work that could be relaxed in future studies.

# 2 Study Site

# 2.1 Description

We use hydrometeorological data and flux measurements from a 25m tall eddy covariance flux tower in the Intensively Managed Landscapes Critical Zone Observatory (IML-CZO), located at 40.155N, 88.578W, Goose Creek Township, Piatt County, Illinois, US

(Figure 1). In the Upper Sangamon River Basin, both glacial and management legacies have shaped soils, topography, and native land cover resulting in a low-relief landscape with poorly drained soils (Kumar et al., 2018; Anders et al., 2018). Therefore, the use of tile-drains is a common practice in the crop fields for subsurface drainage (Wilson et al., 2018). The climate at the study site is humid continental (Koppen climate classification Dfa) with warm and humid summers and cold winters. Historically, maximum precipitation occurs in late spring and early summer (i.e. April to June) with an average of about 100 mm per month (Mishra & Cherkauer, 2010) and long-term observations have shown that Illinois has become wetter during the crop-growing season (Mishra & Cherkauer, 2010).

In this agricultural landscape, vegetation dynamics are a strong determinant of landatmosphere fluxes and their seasonality in the landscape. These dynamics are highly influenced by crop rotation between maize and soybean fields every one or two years, which is a prevalent practice, along with different intensities of tillage (Wilson et al., 2018). The region has a return of one harvest per year. Planting occurs from early April to late May, and harvest occurs from late September to early November. Maize is typically planted before soybean and harvested after, such that it has a longer growing season (NASS, 2010). In this study, we consider an April-March window as a "crop year" (e.g. April 2016 to March 2017 is denominated in this study as "crop year 2016"). Both crops have a peak vegetation cover with very dense leaf area index (LAI) reaching 4 for maize and 6 to 7 for soybean (Drewry et al., 2010). A distinctive feature of this agricultural region is how the dense vegetation cover during the growing season contrasts drastically with the almost bare landscape left after harvest until the following spring season when planting occurs (NASS, 2010) (Figure 2). After harvest, crop residues, i.e., mainly litter, stover and plant roots, remain on the surface and in the shallow soil layers until the following spring when planting occurs (Warner et al., 1989).

#### 2.2 Instrumentation and Data

165

166

167

168

169

170

171

172

173

174

175

176

177

178

179

180

181

182

183

184

186

187

188

189

190

191

192

193

196

Our 25m-tall eddy covariance flux tower sees the combined response of hundred of different plots every 15-min in the "patchwork quilt" landscape inside its several square kilometers size dynamic flux footprint. We use a set of detailed land cover maps (NASS, 2016-2018) to characterize the annually varying spatial land cover composition. Although the underlying vegetation is non homogeneous, the tower is situated on terrain that is generally flat in all directions for an extended distance upwind, making the study site ideal

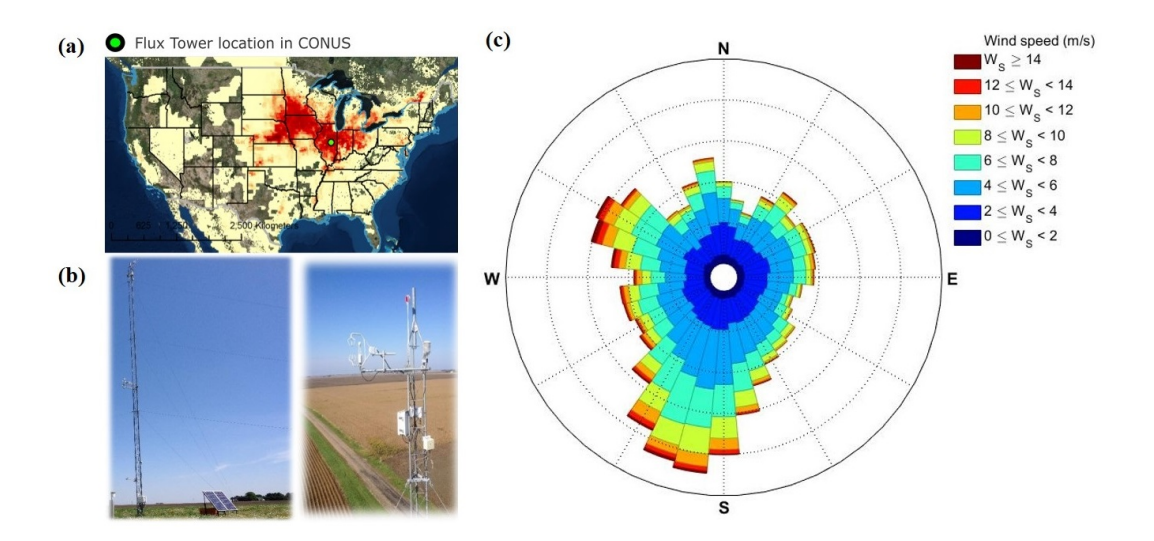


Figure 1. Goose Creek flux tower location and components. (a) Location of the tower (green dot) and the intensity of maize cultivation (the red area represents the corn harvested area fraction (high=red, low= light ivory), (Monfreda et al., 2008)). (b) Fluxes measured by the 25m tall eddy covariance tower come from the underlying heterogeneous landscape consisting of a mosaic of maize and soybean fields, from a fetch that can reach up to 10 km upwind from the tower. (c) The prevailing wind direction is from the southwest (4/23/2016-4/30/2019). The relative frequency with which the wind blows from a particular direction is proportional to the spoke's length, and colors indicate different wind speed categories.

to explore land-atmosphere fluxes dynamics resulting from land cover changes in a human-induced agricultural landscape. The eddy covariance tower has recorded data from April 2016 to present day. The high-frequency instruments that estimate fluxes from the ecosystem are deployed at 25m height (Li-7500 Infrared Gas Analyzer manufactured by LiCor Inc., and CSAT3 Sonic Anemometer manufactured by Campbell Scientific Ltd) (See Supplemental Information Section 1 and Table S1). These instruments sample at 10 Hz and are set to record 15 minute averages. They point to the southwest, the prevailing wind direction (Figure 1). However, constantly shifting wind directions with meteorological conditions have implications for this study (described in detail in Section 3). For more information on the variables used in the analysis and instrumentation at this flux tower, we refer the reader to Supplemental Information Section 1 and Table S1.

# 3 Methods

197

198

199

201

203

204

205

206

207

208

210

Here we describe how we estimate the relative contribution of different land cover types to land-atmosphere fluxes measured at the flux tower. First, we use the wind data to obtain



Figure 2. Panoramic view of the intensively managed agricultural study site. (a) During the growing season in July 2015, a row crop agriculture mosaic dominates the landscape, masking features such as micro-topographic depressions and soil variability. The vegetated land cover connects the heterogeneous ecosystem and the overlaying atmosphere during the growing season. (b) Right after harvest (October 2017), only litter remains over the surface. "R" marks a common reference point between the two pictures (Photo credit: (a) Allison Goodwell, (b) Leila Hernandez Rodriguez).

the variability of the areal coverage by using a two-dimensional flux footprint parameterization. Then we use a process-based ecohydrological model to obtain the temporally varying ratio of the flux values for different land covers. We use both the observed data and the modeled ratio of fluxes to estimate the contribution of each crop to the observed fluxes. From this, we can characterize the patterns of magnitude and variability of fluxes. Knowing that the observed fluxes at the ecosystem scale also carry the influence of the spatial heterogeneity within the flux footprint, we deconvolve the signal of the eddy covariance observation by quantifying the differential weighting of the plots based on the land cover types inside its dynamic flux footprint to find the relative contribution of each land cover type on the observations.

# 3.1 Estimation of two-dimensional flux footprint

Latent heat (LE), sensible heat, (H), and  $CO_2$  fluxes  $(F_c)$  estimated by the flux tower at any given time point correspond to an uncertain origin on the landscape. This origin can be estimated as the flux footprint, which is defined as the upwind landscape area that contributes to the measured vertical flux or concentration at a specific time (Vesala et al., 2008; Burba, 2013; Kljun et al., 2015). In this study, we use the two-dimensional

flux footprint prediction model (FFP) proposed by Kljun et al. (2015), which considers the effects of surface roughness, atmospheric stability, and the crosswind spread of the footprint. For an agricultural landscape, surface roughness length changes as a function of vegetation height through the growing season. Also, atmospheric thermal stability rapidly changes with air temperature and density at a given pressure, impacting the vertical motion of air parcels. As a result, the areal contribution associated with each land cover type changes dynamically. The FFP model provides the width and shape of the two-dimensional flux footprint at any give time, where the source/sink area of the fluxes is located on the horizontal surface (x, y), and the tower height in the vertical direction, z (Figure 3). The FFP model assumes stationarity over the eddy-covariance integration period (here, 15-min) and horizontal homogeneity of the flow, but not of the scalar source/sink distribution.

When estimating the two-dimensional flux footprint, at each time interval the observed fluxes have their origin in a different combination of maize or soybean fields. To derive the source area up to a certain percent of flux contribution, we define a set of five contours (r) that define the areas that contribute 20, 40, 60, 80, and 90% of the total flux estimated by the flux tower. At farther locations beyond  $r_{90\%}$  that correspond to a contribution of 90%, the contributions tail off, so we limit our study to  $r_{90\%}$  (we use  $r_{\%}$  or r to represent percentage or equivalent fractional contribution, respectively). The associated fetch changes direction and length at every time step. In this context, the fetch is the distance from the tower to a specific fraction of the flux contribution. For example, the fetch for a 50% contribution  $(r_{50\%})$  will be shorter than for a 90% contribution  $(r_{90\%})$  (Burba, 2013).

We used the FFP model as a function on a loop in our Python code to estimate flux footprints for each 15-min data point from April 2016 to April 2019. Here we describe the inputs required for the FFP model. The calculation of the boundary layer height, blh, is based on the bulk Richardson number,  $R_i$ , method (Vogelezang & Holtslag, 1996) which is suitable for convective and stable boundary layer conditions and has been used in several previous studies (Lee & De Wekker, 2016; Seidel et al., 2012). We used the blh retrieved from the fifth generation reanalysis dataset for the global climate and weather, ERA5 (ECMWF, 2018) from the European Centre for Medium-Range Weather Forecasts (ECMWF). Near-surface atmospheric turbulence is caused by thermal and mechanical effects. Thermal turbulence is produced by temperature gradients and buoyant forces, while the mechanical turbulence is generated by friction forces driven by wind shear, and therefore both control atmospheric fluxes. To account for atmospheric stability we calculate the Obukhov length, L, (Foken,

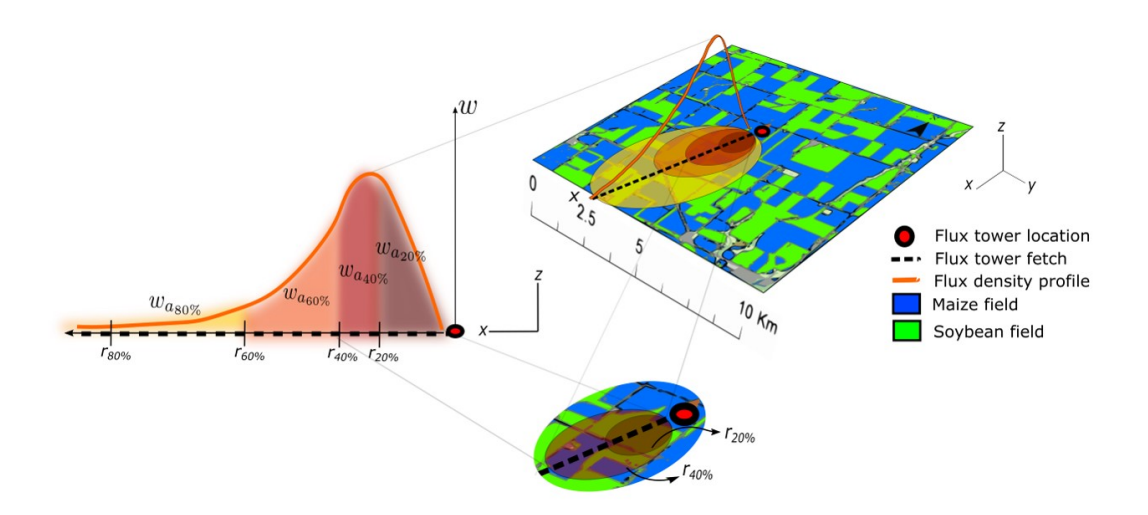


Figure 3. Illustration of a two-dimensional flux footprint that captures the organized heterogeneity of the maize-soybean mosaic. The land cover data from USDA 2016 (right) shows a mosaic of maize and soybean surrounding the flux tower. The density profile over the mosaic (orange) represents the relative contribution of the flux footprint as a function of the upwind distance, denominated as the fetch (black dashed line). The density profile shows that higher contributions come from locations close to the tower, but not immediately underneath. In the two-dimensional approach (Kljun et al., 2015) the area defined by a set of contours  $(r_{\%})$  of increased percentage of contribution (bottom) define the strength and location of the sources/sink areas that contribute to the flux estimated at the tower. w is the weighted flux footprint contribution of each patch of area (a) defined by a given contour. Therefore, the flux tower measurement is the combined response of the fields inside the flux footprint (left).

2006), which is positive for stable and negative for unstable atmospheric stratification, and becomes near-infinite in the limit of neutral stratification. Finally, the last input to the FFP model corresponds to the standard deviation of the lateral velocity fluctuations,  $\sigma_v$ , which is estimated using the 15-minute root-mean-square of the cross main-wind component, v, from the high-frequency data at the flux tower. The displacement height, d, is defined as the distance above the ground at which a non-vegetated surface should be placed to provide a logarithmic wind field equal to the observed one (Stull, 2012). We estimated the variation of d during the growing season as a function of the average height of maize,  $d = 0.67 * h_m$  (Jacobs & Van Boxel, 1988). The variation of canopy height and LAI has been proven to be nearly simultaneous in crops like maize (Gao et al., 2013; Alekseychik et al., 2017), therefore we used LAI as a proxy to define the average changes of height of the crops in the region. The measurement height above displacement height,  $z_m$ , is calculated as  $z_m = z - d$ , where z = 25m is the tower height and d the displacement height.

#### 3.2 Heterogeneity and flux partitioning equations

Here we describe the approach to estimate the relative flux contribution due to heterogeneous land cover. Analytically, the distribution of a diffusive quantity in the lower layer of the atmospheric boundary layer is described as an integral diffusion equation. Therefore, the flux footprint relates the vertical eddy flux  $\eta$  from a flux tower located at the origin (0,0) and with an observation height,  $z_{obs}$ , to the spatial distribution of ground source (or sink) fluxes  $\mathscr{F}(x,y)$  at the ground (z=0) at a upwind distance (x) and crosswind (y) direction from the tower location (Pasquill & Smith, 1983; Schuepp et al., 1990; Horst & Weil, 1992; Schmid, 1994; Vesala et al., 2008):

$$\eta(0, 0, z_{obs}) = \int_{\mathscr{R}} \mathscr{F}(x, y) \cdot \omega(x, y) dx dy \tag{1}$$

where  $\mathscr{R}$  denotes the flux footprint and  $\omega(x,y)$  is the relative contribution to the flux at any location (x,y) (Kljun et al., 2015).  $\mathscr{F}(x,y)$  is the source (or sink) flux from the surface at location (x,y), with the same units as  $\eta$ , where  $\eta = \eta(0,0,z_{obs})$ . The observed flux  $\eta$  is then the weighted integration of all the surface fluxes inside the contour  $r_{90\%}$  of flux contribution, and has units of  $W/m^2$  for latent heat flux, LE, and sensible heat flux, H, and  $\mu mol/m^2s$  for  $CO_2$  flux,  $F_c$ . This approach assumes that the turbulent flow field is horizontally homogeneous (Horst & Weil, 1992). Consequently, the relative contribution of each field source or sink is a function of its location within the flux footprint.

We assume that fluxes are the same within a given patch of a crop, and there are n landscape patches that contribute to the measured flux inside the flux footprint. To account for a measure of surface heterogeneity, the source emission or sink rate for n different sources (or sinks) Equation (1) is expressed as:

$$\eta = \sum_{i=1}^{n} F_i \cdot w_i \tag{2}$$

where  $F_i$  is the ground level flux for patch i and  $w_i$  is the weighted flux footprint contribution of each patch of area  $a_i$  located inside the contour described by any given fraction of contribution from a defined set of contours r. We can account separately for the weighted flux footprint from maize and soybean fields, represented by the subscripts m and s, inside each contour respectively, as follows:

$$w_{m_i} = A_m \cdot r \quad \text{and} \quad w_{s_i} = A_s \cdot r$$
 (3)

where the total fraction of the area covered by maize and soybean inside a contour can be denoted by  $A_m$  and  $A_s$ , respectively, as follows:

$$A_m = \frac{\sum_{\forall i \in m} a_i}{a_T}$$
 ,  $A_s = \frac{\sum_{\forall i \in s} a_i}{a_T}$  , and  $a_T = \sum_i a_i$  (4)

where we can aggregate the patch areas  $a_i$  by adding the contributions of each patch type and the total area is  $a_T$ . Here we assume that the fluxes are the same for all patches of a given crop type, such that we can aggregate those patches to compute the relative contribution of each crop/land cover type by summing the contributions as follows:

$$\phi_m = \sum_{\forall i \in m} w_i \quad \text{and} \quad \phi_s = \sum_{\forall i \in s} w_i$$
 (5)

where the subscripts m and s refer to maize and soybean, respectively. We now assume that one "crop" flux value for all maize as  $C_m$ , and for all soybean as  $C_s$ . This constitutes the assumption that the vegetation type is the dominant source of flux variability, and ignores influences such as soil moisture or nutrients along the fetch. This assumption could be relaxed if detailed characteristics of each landscape patch were available. As described in the next subsection, we use a multilayer canopy model to estimate the vegetation-level fluxes  $(LE, H, F_c)$  for each crop type. Since these fluxes are modeled, here denoted as  $C_m$  and  $C_s$  for maize and soybean, respectively, their application to Equation (2) results in a total "modeled" flux  $\eta_{mod}$ :

$$\eta_{mod} = C_m \phi_m + C_s \phi_s \tag{6}$$

Due to these simplifying assumptions, model error, and observation errors, we expect  $\eta_{mod}$  to be different from the observed tower flux,  $\eta$ . Therefore, our aim is not to validate our modeled results against flux observations, but to merge flux tower observations, and models to improve the crop-specific estimates. Lastly, we compute the partitions of the fluxes observed at the tower for maize and soybean fields, respectively, as follows:

$$\eta_m = \eta \cdot \frac{C_m \cdot \phi_m}{\eta_{mod}} = \eta \cdot \frac{C_m \cdot \phi_m}{C_m \cdot \phi_m + C_s \cdot \phi_s} \tag{7}$$

$$\eta_s = \eta \cdot \frac{C_s \cdot \phi_s}{\eta_{mod}} = \eta \cdot \frac{C_s \cdot \phi_s}{C_m \cdot \phi_m + C_s \cdot \phi_s}.$$
 (8)

Based on this, we combine the relative fluxes from a process-based model with a twodimensional footprint model to determine both the fractional and actual contributions to the flux.

#### 3.3 Ecohydrological modeling to simulate maize and soybean behavior

We use an annual land cover product from the United States Department of Agriculture (USDA) Cropland Data Layer (CDL) at 30m spatial resolution (Figure 3) to determine land cover in each footprint. Some fields see maize-soybean rotation while others see maize-maize-soybean rotation. We assume that the land cover for a year does not change until the planting the next year, and therefore define a single land cover from April through March of the next year, a "crop year". We use Equation (5) to compute the flux footprint contribution for maize and soybean,  $\phi_m$  and  $\phi_s$  respectively.

We use the well-tested and validated Multi-Layer Canopy model, MLCan (Drewry et al., 2010; Le et al., 2012), to simulate the flux response of maize and soybean,  $C_m$  and  $C_s$  respectively, under observed atmospheric drivers. MLCan uses a multilayer discretization of the canopy and root zone, including a litter layer on the soil surface, to simulate the below- and above-ground ecohydrological processes for different vegetation types. At the leaf scale, ecophysiological (photosynthesis and stomatal conductance) and physical (leaf-boundary layer conductance and energy balance) components are coupled to determine flux densities of  $CO_2$ , and latent and sensible heat, and then integrated to the canopy scale. For an extended description of the model and its validation for maize and soybean we refer to Drewry et al. (2010).

We compute the fluxes associated with maize and soybean, which use C4 and C3 photosynthetic pathways, respectively. The model is driven by above-canopy measurements of air temperature  $(Ta)[{}^{\circ}C]$ , barometric pressure (Pa)[kPa], global solar radiation (i.e. incident shortwave radiation)  $(Rg)[W/m^2]$ , precipitation (PPT)[mm], and vapor pressure

deficit (VPD)[kPa] from April 2016 to March 2019. Leaf Area Index (LAI) was obtained from the Moderate Resolution Imaging Spectroradiometer (MODIS) 8-day dataset at 500m resolution (Myneni et al., 2015). Pixels around the tower that contained a single crop were selected to estimate maize and soybean LAI. Satellite LAI measurements were complemented with LAI estimates from field measurements of Normalized Difference Vegetation Index (NDVI) calculated as described by Nguy-Robertson et al. (2012). LAI is assumed to be zero during the non-growing season, when no vegetation is on the surface and only litter from the previous season's crops remain. Maize and soybean parameters for the model are provided in SI Table S2. MLCan simulations provide LE, H, and  $F_c$  at 15 minute resolution for maize  $(C_m)$  and soybean  $(C_s)$ . These are then used to compute the total modeled flux and relative contributions (Equation (6)).

## 3.4 Illustration of the role of organized heterogeneity

345

346

347

348

349

350

351

354

355

356

357

358

359

360

361

362

365

366

367

368

369

370

371

372 373

374

375

At a single time step, we consider that the total contributions of the flux footprint from maize and soybean ( $\phi_m$  and  $\phi_s$  respectively) are defined by the sum of their relative contributions (Figure 4), as expressed in Equation (5). As an illustrative example, we consider three cases (Figure 4, Table 1) where  $\phi_s = \phi_m = 0.5$  (Case A),  $\phi_s = 0.4$  and  $\phi_m = 0.6$ (Case B), and  $\phi_s$ =0.6 and  $\phi_m$ =0.4 (Case C). Case A corresponds to equal contributions from the two crops as would be expected if the two were randomly distributed or the organized heterogeneity incidentally reflected equal contributions, like in the hypothetical case shown in Figure 4a. Cases B and C reflect relatively larger contributions from maize or soybean, respectively. For all three cases, assume we know that the modeled fluxes are  $LE_s=120$  $W/m^2$  and  $LE_m=80$   $W/m^2$ , and the tower observed flux is  $\eta=105$   $W/m^2$ . For Case A this leads to a total estimated flux  $n_{mod} = 100 \ W/m^2 (= (.5)120 + (.5)80)$ . For Cases B and C, we would estimate  $n_{mod}$  as 96  $W/m^2$  and 104  $W/m^2$ , respectively. Since for all three cases, the observed flux at the tower is the same, we can estimate the difference between  $\eta$  and  $\eta_{mod}$  (Table 1). In this example, we see that the landscape heterogeneity of Case C leads to the closest estimate to the flux measured at the tower. We can also consider the percent difference in  $\eta_{mod}$  relative to the equal contributions of Case A. Here, we see that Case B leads to a -4% difference in *LE*, due to the higher contribution from maize, which has a lower LE. The opposite occurs for Case C (Table 1).

This example also demonstrates that the change in the relative contribution of fluxes due to two crop species can either increase or decrease the total flux observed at the tower

**Table 1.** Comparison between the random and organized heterogeneous mosaic cases (Figure 4) towards the estimation of latent heat flux,  $\eta \equiv LE$ . Case A refers to the "equal contribution assumption" (Figure 4a), whereas Case B (Figure 4b) & Case C are heterogeneous situations in which soybean and maize are more dominant, respectively.

Case	$\eta(\text{LE})$	$\phi_s$	$\phi_m$	$LE_s$	$LE_m$	$\eta_{mod}$	$\eta$ - $\eta_{mod}$	diff from A
	$W/m^2$	frac	frac	$W/m^2$	$W/m^2$	$W/m^2$	$W/m^2$	%
A	105	0.5	0.5	120	80	100	5	0
В	105	0.4	0.6	120	80	96	9	-4
$\mathbf{C}$	105	0.6	0.4	120	80	104	1	4

 $(\eta)$  relative to the hypothetical case of a random distribution of crops. In other words, an incremental change in flux observed at a tower could either correlate to a change in flux from the crops or a shift in relative land cover contributions. This has significant implications for flux tower data interpretation in a heterogeneous landscape.

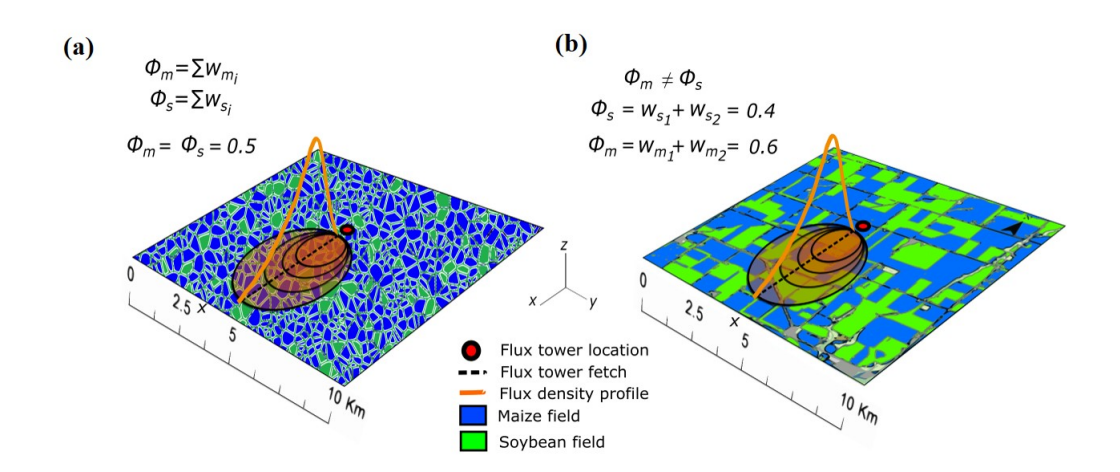


Figure 4. Conceptual illustration of the flux footprint responses of (a) a random land cover mosaic where maize and soybean equally contributes to the total observed flux  $(\phi_m = \phi_s = 0.5)$ , and (b) an organized heterogeneous land cover mosaic as observed at the study site.

# 4 Results and Discussion

376

377

378

379

381

382

# 4.1 Ecosystem fluxes dictated by agricultural management

To understand the general behavior of the study site, we analyze all 15 min data from 23 April 2016 to 15 April 2019 in terms of average diurnal ecosystem fluxes within the flux footprint. H and LE both peak at midday as expected (Figures 5a and b), and negative

386

387

388

389

390

391

392

393

397

398

399

400

401

402

403

406

407

408

409

410

411

412

413

414

415

416

values of  $CO_2$  flux,  $F_c$ , during the daytime reflect ecosystem uptake due to photosynthesis (Figure 5c). This absorbed  $CO_2$  can be fixed by plants to form tissue, remain in the soil as litter and roots, or leave the system through lateral soil movement or harvested grain. Positive values of  $F_c$  during nighttime reflect a combination of autotrophic and heterotrophic respiration. We found that annually, the agricultural system acts as a sink for  $CO_2$ , with negative  $CO_2$  annual budgets during a "crop year" (Table 2). Our analysis also shows that crops evapotranspire on average 72% of the total annual ET during the growing season.

The difference in the net  $F_c$  ( $CO_2$  released minus  $CO_2$  uptaked by the ecosystem) between the three crop years (Table 2) is assumed to be primarily influenced by two sets of factors: (1) hydroclimatological drivers acting on the ecosystem, such as precipitation (PPT) and radiation; and (2) the difference in the fraction of maize and soybean in the flux footprint due to the organized heterogeneity of the ecosystem. Here we evaluate the former factor, while the latter, which is the main focus of this study, is discussed in the following subsections. Specifically, in Subsection 4.5, we discuss the interpretation of the behavior of the observed net  $F_c$  and its relationship with the contribution of each land cover type. For the first factor, we examined the cumulative rainfall during the crop growth period (Figure 5g), which shows differences across the three years. The lowest accumulated precipitation is observed for the 2017 growing season, followed by 2018 and 2016. This reveals an opposing relationship between cumulative growing season rainfall and annual  $CO_2$  uptake, since the 2017 growing season corresponds to the highest  $CO_2$  uptake (Table 2). Initially, these results seem to contradict the notion that increased precipitation helps carbon uptake (Nemani et al., 2002). Therefore, we investigate the relationship between PPT, LE, and  $CO_2$  flux  $(F_c)$  at the intra-annual basis (Figure 6c). During non-growing season months net  $F_c$  is positive, meaning more  $CO_2$  is released rather than taken up by the system. Also, right after harvest,  $CO_2$  is no longer taken up by crops and a release of  $CO_2$  is expected from crop residues due to the organic matter decomposition of stover and roots that remains in the field (Yan et al., 2019). On the other hand, more  $CO_2$  is taken up during the growing season than released to the atmosphere and therefore  $F_c$  is negative. During non-growing season LE corresponds to soil evaporation, and  $F_c$  corresponds to respiration, both of which are very low. For this system, average monthly LE is limited to an upper threshold of about  $100 \ W/m^2$ , controlled by solar radiation (Figure 6c). However, we observe a difference in the diurnal behavior of the inter-annual variability of the Bowen ratio (H/LE) (Figure 5f).

For the years of analysis, the Bowen ratio is less than 1, indicating that the system is not water limited at the annual scale.

417

418

419

420

421

422

423

424

425

429

430

431

432

433

434

435

436

437

438

439

440

441

442

443

Since vegetation growth stages heavily influence land-atmosphere exchange dynamics, we explored the intra-annual evolution of the daily average behavior using 6-week windows for LE, H (Figure 6a, blue and orange lines, respectively) and  $F_c$  (Figure 6b). The intraannual dynamics of the net  $CO_2$  flux (Figure 6c) shows the windows when  $CO_2$  uptake (negative value) is prevalent. We observe the coupled behavior of  $F_c$  and LE, for when  $CO_2$  uptake higher LE also peaks, which means that water is evapotranspired at a higher rate. During the period of this analysis, the highest  $CO_2$  uptake is observed from July 16 to August 31, 2017 (Figure 6c, window 11), the time of year when crop growth peaks. Soil respiration might be positively related to precipitation and soil temperature (Lei & Han, 2020; Birch, 1958). Therefore, a lower cumulative rainfall in 2017 may have contributed to a lower soil respiration rate in comparison with 2016 and 2018 (e.g. Figure 6c, shows lower  $CO_2$  release in window 12 than in windows 4 and 20). Consequently, both a high  $CO_2$  uptake during the growing season and low  $CO_2$  release during the non-growing season contributed to the high net  $CO_2$  uptake in 2017. As observed at seasonal time-scales, the non-stationary behavior of LE and  $CO_2$  fluxes reveal a human-induced trend in which the imposed land cover controls the energy and  $CO_2$  exchange between the land-surface and the atmosphere. Consequently, the effect of vegetation on  $F_c$  is relevant, and, therefore, we quantify the relative contribution of each crop type to determine the origin of the higher  $CO_2$  uptake observed by the tower during 2017 (See Subsection 4.5).

**Table 2.** Annual  $CO_2$  budget and mean  $CO_2$  concentration inside the flux footprint

Crop year	2016	2017	2018
Net $CO_2$ budget $(kg/m^2)$	-0.15	-0.57	-0.23
Avg $CO_2$ conc $(ppm)$	409.16	407.02	409.84

# 4.2 Flux footprints cover a wide range of landscape areas

The size of the flux footprint strongly depends on the highly variable atmospheric stability at the sub-hourly time scale. At the annual scale or for observations over long periods, the effect of the atmospheric stability on the footprint climatology, or average footprint, is weaker (Kljun et al., 2015; Zhang & Wen, 2015; Tuovinen et al., 2019). The changes on the climatological footprint for crop years 2016 (Figure 7a), 2017 (Figure 7c),

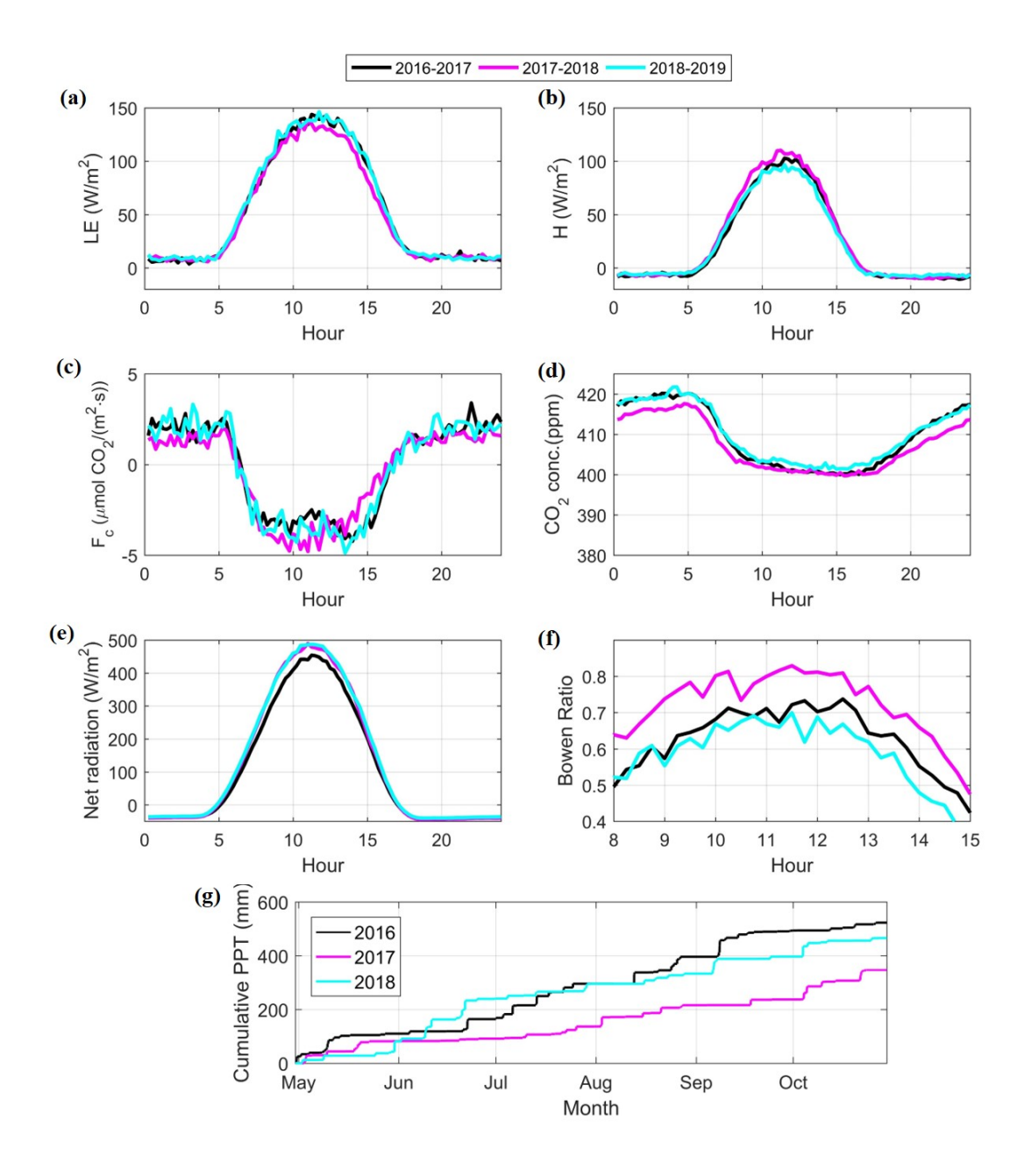


Figure 5. Daily averaged observations of atmospheric fluxes and radiation, and inter-annual rainfall at the study site (a), for crop year 2016 (i.e. April 2016 to March 2017) (black lines), crop year 2017 (magenta lines), and crop year 2018 (cyan lines), for: (a) Latent heat flux, LE; (b) Sensible heat flux, H; (c) Net  $F_c$  ( $CO_2$  emitted minus uptaken by the system); (d) Carbon dioxide concentration; (e) Net radiation; (f) Bowen ratio (H/LE); and (g) cumulative rainfall for the growing seasons 2016, 2017 and 2018.

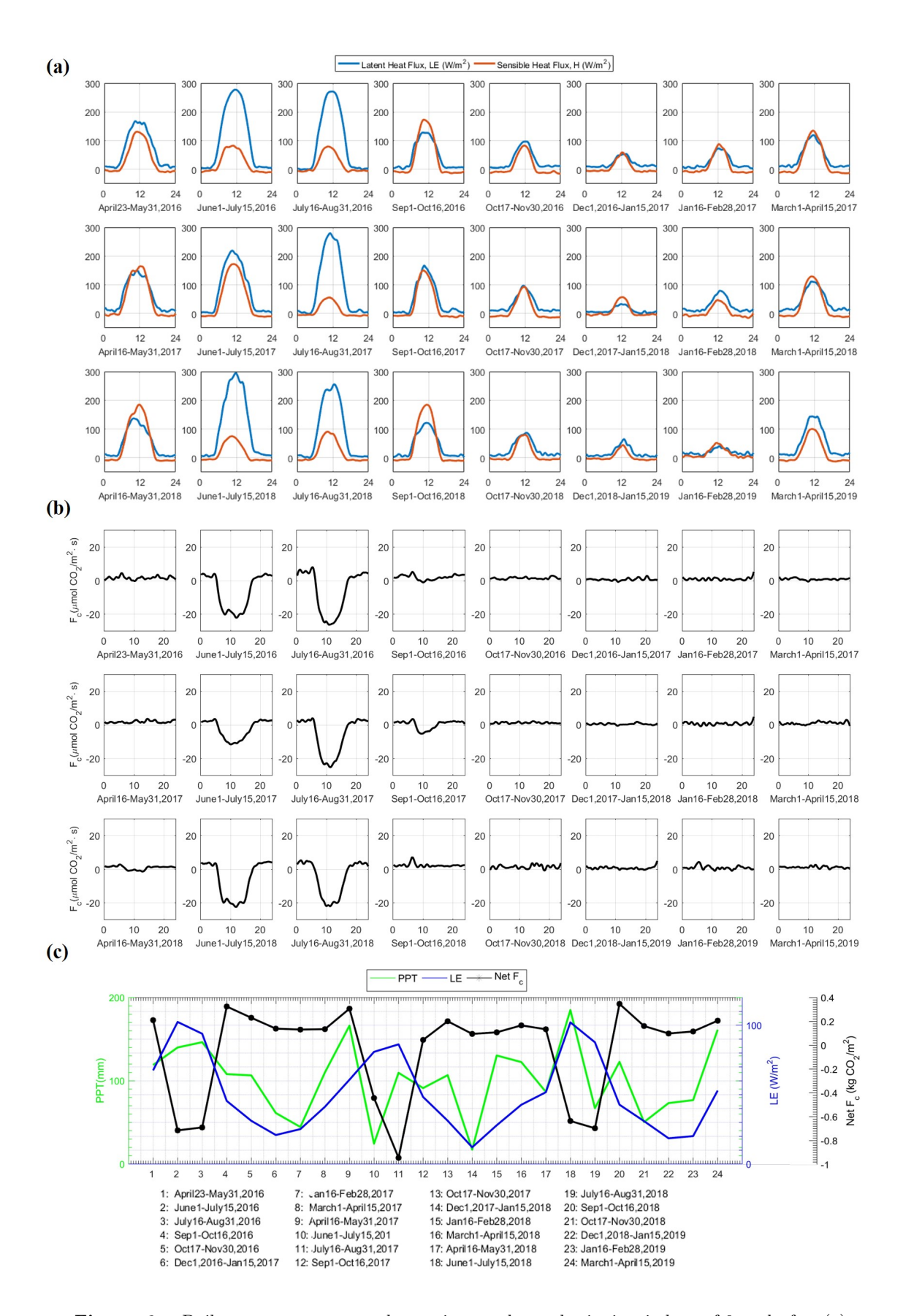


Figure 6. Daily average ecosystem observations at the study site in windows of 6-weeks for: (a) latent and sensible heat flux, LE and H; and (b) carbon dioxide flux,  $F_c$ . (c) Net  $F_c$ , average LE, and total precipitation PPT, for April 2016 - April 2019.

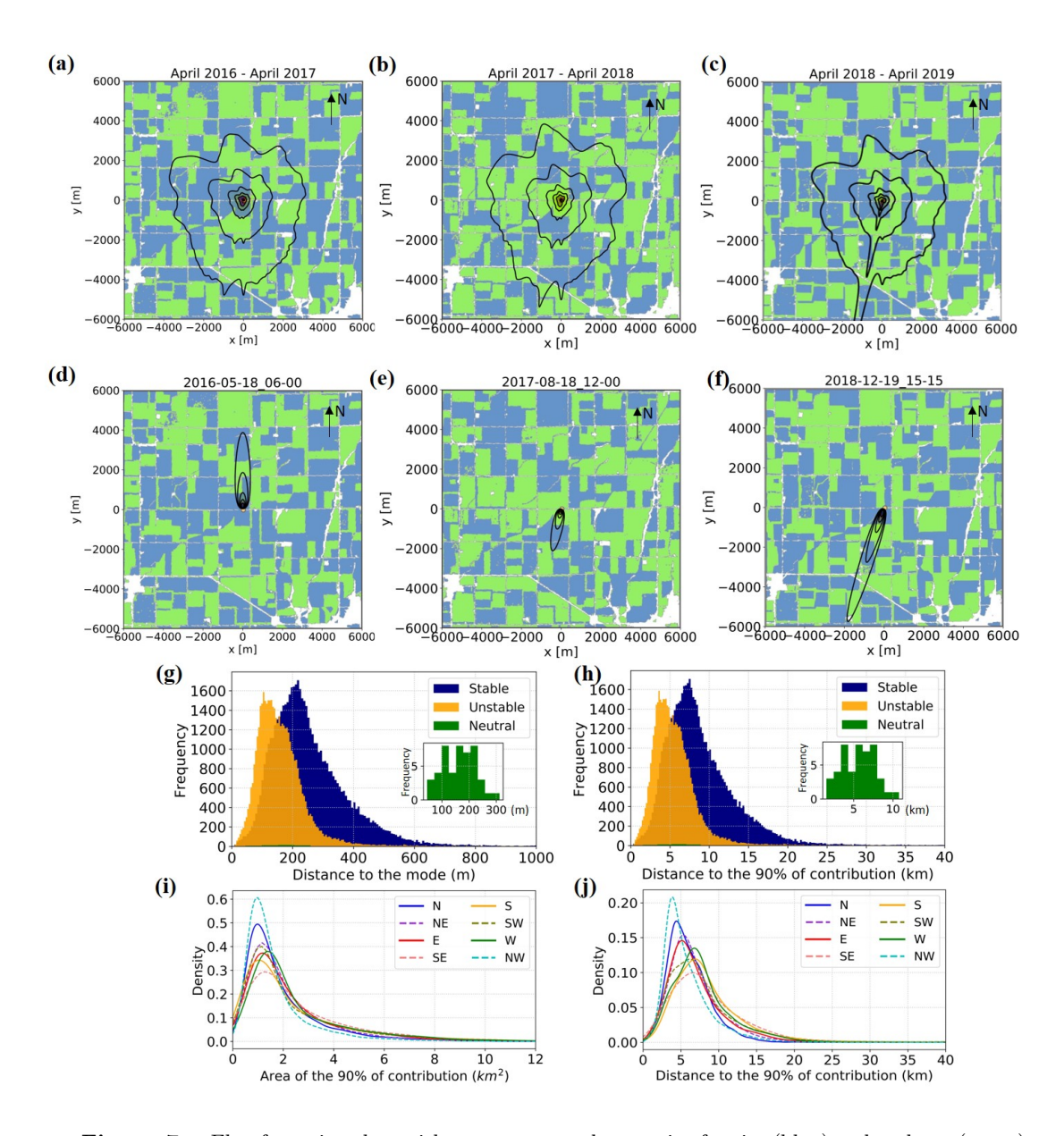


Figure 7. Flux footprint plots with contours over the mosaic of maize (blue) and soybean (green) crops with the center at the flux tower. Each flux footprint plot shows the source area defined by the contours of 20, 40, 60, 80, and 90% (outer contour) of the total flux contribution. The climatological (or average) flux footprint for crop years (a) 2016 (i.e. April 2016 to March 2017), (b) 2017, and (c) 2018, correspond to the aggregation of all single footprints over the year. A sample of single 15-minutes averaged flux footprints under (d) neutral  $(05/18/2016\ 06:00)$ , (e) unstable  $(08/18/2017\ 12:00)$ , and (f) stable  $(12/19/2018\ 15:15)$  atmospheric conditions show the changes in size and location of the source area of the surface flux defined by the dynamic flux footprint. Histograms of the 15-min FFP analysis for the upwind distance (fetch) to the (g) mode and to the (h) 90% of flux contribution, illustrate the average behavior under stable (blue), unstable (orange), and neutral (green) atmospheric conditions over the 3 years of analysis. The probability density function of the upwind (i) area and (j) distance of the 90% of flux contribution show differences based on wind direction.

and 2018 (Figure 7e) show that the mean fetch for  $r_{90\%}$  is approximately 3km. A sample of flux footprints under neutral (Figure 7a), unstable (Figure 7c) and, stable (Figure 7e) atmospheric conditions show the different size of the flux footprint contours for each case. Turbulent mixing plays an important role in the magnitude of fields' relative contributions, as the weighting of fields farther away from the tower increases with increasing stability. In general, the flux footprint size decreases with decreasing  $z_m/L$  (Subsection 3.1). Therefore, under unstable conditions (Figure 7d) we can expect a smaller flux footprint than under stable conditions (Figure 7f).

We found that the average distance to the flux footprint peak is 168m for unstable conditions and 268m for stable conditions (Figure 7g). Therefore, the fields of peak flux contribution are located in between those distances. The footprint is wider as the standard deviation of the lateral wind fluctuations increases and, therefore, the crosswind dispersion increases (Zhang & Wen, 2015; Kljun et al., 2015). On average, the upwind area described by the contour of the 90% of contribution corresponds to  $1.51km^2$  for unstable conditions and  $3.17km^2$  under stable conditions. Similarly, the upwind distance to the contour described by the 90% of the flux contribution for unstable conditions is closer than for stable conditions, with 5.8km and 9.2km, respectively (Figure 7h). The implications of these results for the partitioning of flux contributions for each crop type due to the flux footprint are discussed in the following subsections.

#### 4.3 MLCan distinguishes between maize and soybean fluxes

We used MLCan as described in Subsection 3.3 (Le et al., 2012) to obtain LE, H, and  $F_c$  for maize and soybean, and to explore their intra-annual behavior (Figure 8). From MLCan results, we observe that LE is higher for maize than for soybean (Figure 8a). This occurs for all months except for June to July 2018 when LE is higher for soybean. However, at night, we observe higher condensation rates (or dew formation), in the form of negative LE, for maize relative to soybean.  $CO_2$  uptake patterns by both crops are consistent with the observations at the flux tower (Subsection 4.1), with more uptake of  $CO_2$  by the soil-crop system around noon due to photosynthesis, surpassing respiration (Figure 8b; negative  $F_c$  means the direction of the flux is downwards). At nighttime, positive  $F_c$  is attributed to respiration from the system. Given the dependence between LE and  $F_c$ , we explored their coupled behavior during the growing season (See SI section 4 and Figure S1) and we found

that the four stages -planting, growing, maturing, and harvest- cluster together for maize and soybean.

475

476

477

478

479

480

481

482

486

487

488

489

490

491

492

496

497

498

499

500

501

502

503

506

# 4.4 Flux contributions evolve due to organized heterogeneity and hydroclimatological drivers

We estimated the relative contribution of average daily fluxes of maize and soybean (Figure 9) using the observed flux tower data. The overall trend of LE, H and  $F_c$  exhibit a strong seasonality (Figures 9a, b, and c, respectively). In terms of flux footprint contribution,  $\phi$ , (Figure 9d), a larger contribution from maize fields were observed in 2016 and 2018, when more fields were cultivated with maize in areas between 168m and 268m upwind from the tower. In 2017, soybean was mostly planted in the same fields. However, both crop types influence the magnitude of the observed fluxes. In terms of  $F_c$  behavior across seasons, we observe that a strong release of  $CO_2$  flux into the atmosphere occurs during planting (i.e. starting around mid April) (Figure 9c, numerals 1, 9 and 17) that can be explained by rising temperatures and soil moisture that support heterotrophic respiration of existing biomass on and in the soil. During the peak of the growing season, soybean fields in 2017 contributed more towards a higher  $CO_2$  uptake (Figure 9c, numeral 11), while maize fields in 2016 and 2018 contributed more towards a higher LE (Figure 9c, numeral 2 and 18). Accordingly, this 6-week window analysis shows that maize fields inside the flux footprint contributed more towards daily LE and H than soybean fields during 2016 and 2018 growing season, whereas soybean contributed more than maize in 2017. Therefore, all years have significant contributions from both crops given that the mosaic at a larger scale is different every year (Figure 9).

Next, we explore the seasonal dominance of a given crop type in terms of flux magnitude contribution,  $\phi$ , rather than area contribution. We calculated the difference of the percentage of contribution for the two cases described in Subsection 3.4. First, for the hypothetical randomly distributed mix of plants, in a manner that does not reflect any particular spatial pattern, where the relative contribution of the flux footprint for each crop type is equal,  $\phi_m = \phi_s = 50\%$ . Then, for the relative contribution of each crop from April 2016 to April 2019, where  $\phi_m$  and  $\phi_s$  are unequal and temporally variable (Figure 9). In other words, we want to find what crop is dominant in each window resulting from a combination of fluxes associated with each crop and the fraction they occupy in the flux footprint. To estimate the contribution percentage of each crop, we first calculated the average LE, H, and  $F_c$  for

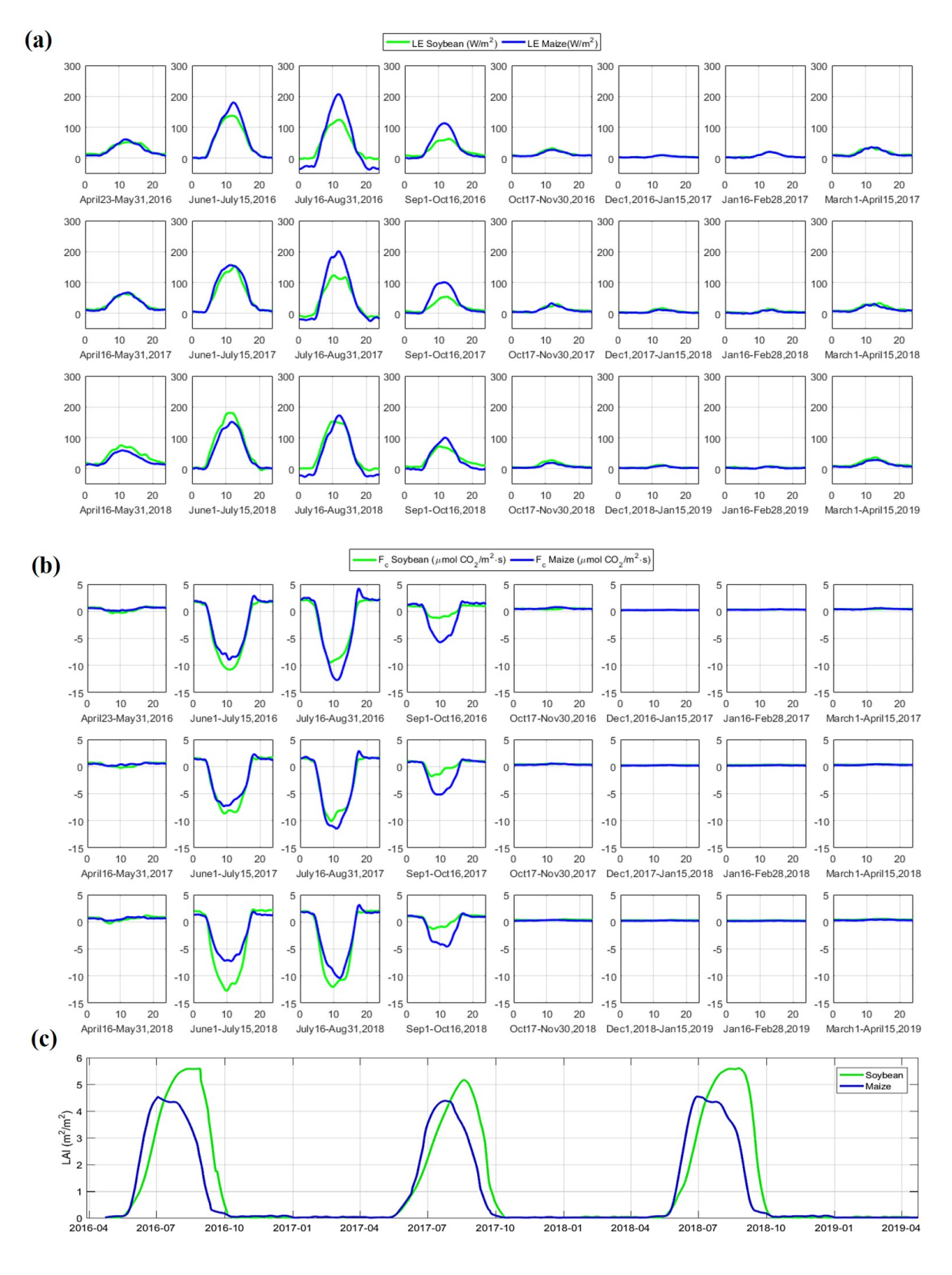


Figure 8. Modeled average daily fluxes of maize (blue) and soybean (green) in 6-week windows: (a) latent heat flux, LE; and (b) carbon dioxide flux,  $F_c$ , using MLCan. Model parameter values are shown in the supplemental material ("MLCan parameters" and Table S2). (c) Canopy leaf area index (LAI) of maize and soybean inside the tower flux footprint for April 2016 - April 2019, estimated as described in Subsection 3.3.

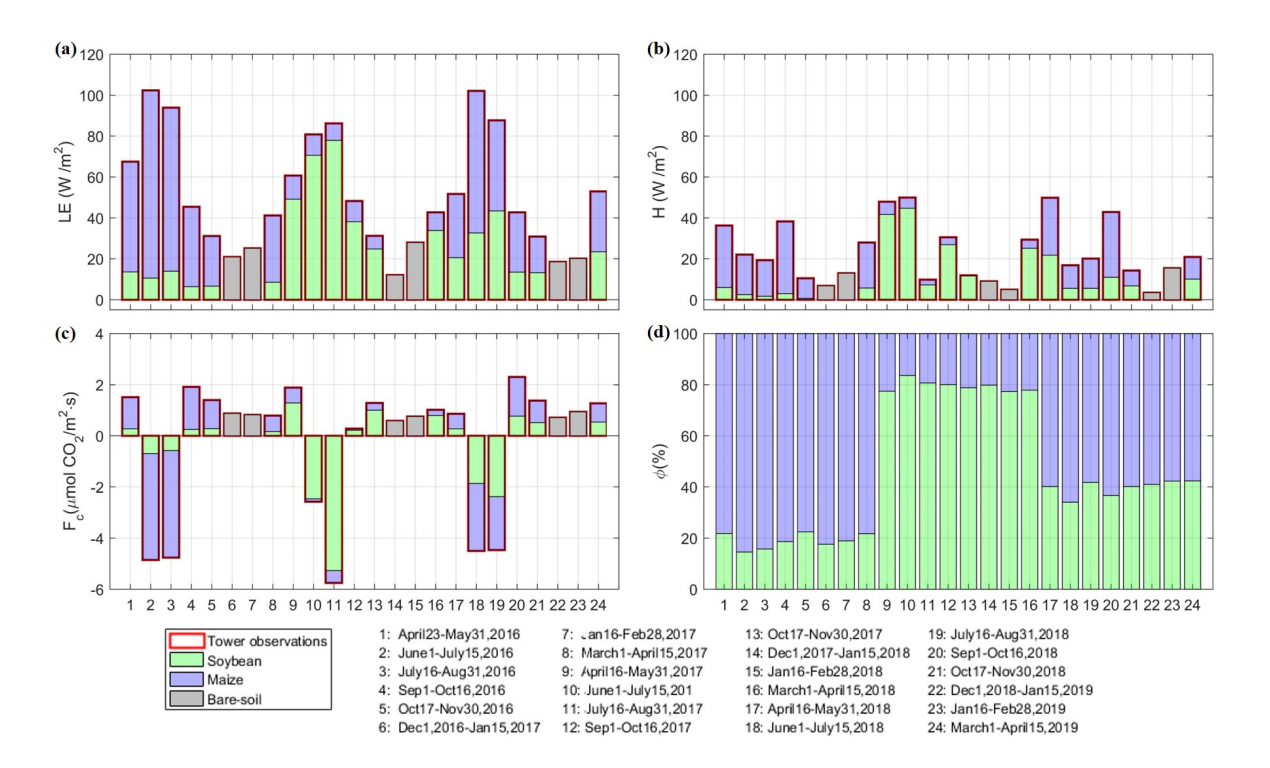


Figure 9. Seasonal evolution of average daily fluxes due to the relative contribution of maize (blue) and soybean (green) in 6-week windows (corresponding to the windows shown in Figure 6), for (a) latent heat flux, LE; (b) sensible heat flux, H; (c) carbon dioxide flux,  $F_c$ ; and (d) relative flux footprint contribution,  $\phi$ . Each stacked bar refers to 6-weeks averaged daily flux for each crop type. Relative contributions due to soybean and maize were calculated with the method described in Section 3 for 15-minute data from April 2016 to April 2019.

508

509

510

511

512

513

514

516

517

518

519

520

521

522

maize and soybean for the 6-week windows, using Equations (6)-(8) and the corresponding  $\phi$  for each case. Then, we subtracted the results assuming random (rather than organized) distribution of crops from the heterogeneous results i.e., organized heterogeneity, to define the dominant crop for each window. The 6-week averaged analysis shows the difference between the percentage of the contributions for the organized heterogeneous mosaic and for the hypothetical random contribution case (Figure 10). While maize fields contributed more to the observed LE and H in crop years 2016 and 2018, soybean fields contributed more in crop year 2017 (Figures 10a and b). The largest effect due to land cover heterogeneity is observed for  $CO_2$  flux ( $F_c$ ) from June 1 to July 15, 2017, (Figure 10c, bar 10), when on an average soybean fields contribution towards  $F_c$  is 24.5% larger than the random case (Figure 10c).

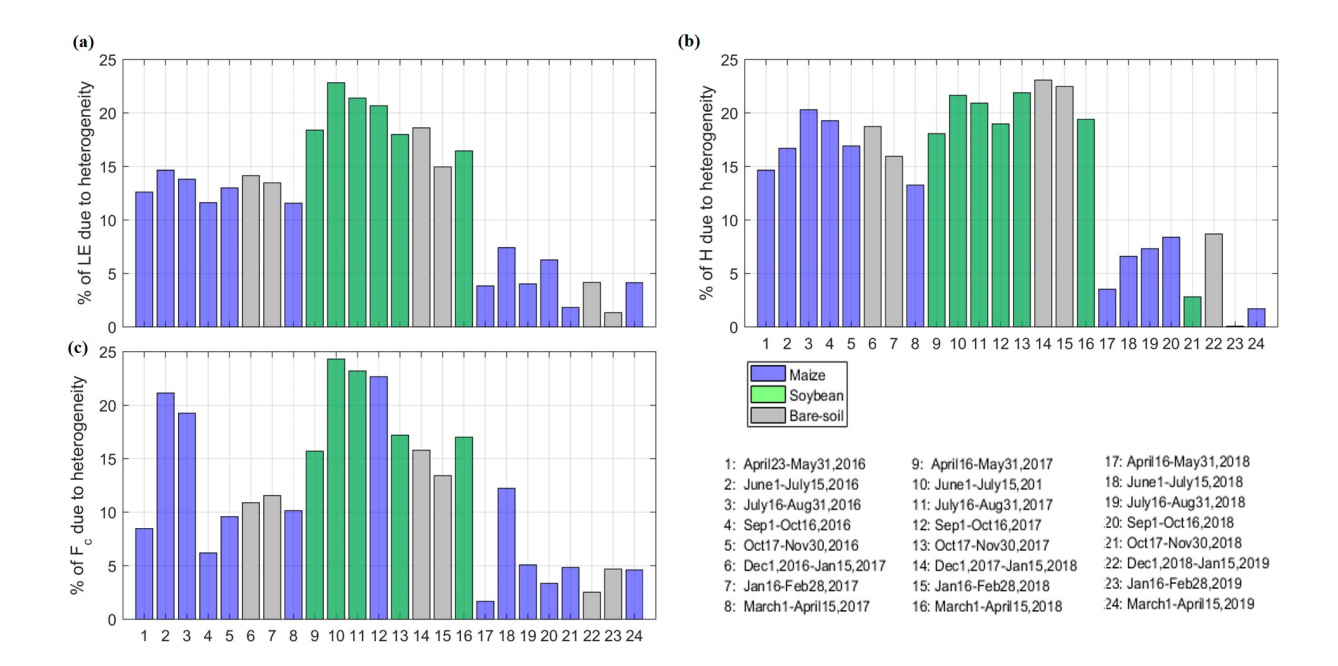


Figure 10. Seasonal evolution of the percent contribution due to organized heterogeneity in 6-week windows (corresponding to Figure 6), for (a) latent heat flux, LE; (b) sensible heat flux, H; and (c) carbon dioxide flux,  $F_c$ . These plots show the difference between the response of a heterogeneous land cover mosaic and a hypothetical random assumption where  $\phi_m = \phi_s = 0.5$ .

Given that the change in flux observed at the tower could either correlate to a change in flux from the crops or a shift in relative land cover contributions, we analyze the effect of the relative contribution due to maize and soybean based on atmospheric conditions (Figure 11). Besides the overall high contribution due to maize and soybean areas nearby the tower under unstable conditions, we observe that maize and soybean show a different

cumulative distribution function based on atmospheric stability. We could have estimated the contribution of individual crops to the total flux observed at the tower at each period using a statistical approach to deconvolve the contributions from different types of vegetation. However, we would require a large amount of data to not lose resolution at times when the flux tower only observes a small area of a certain field (e.g., if the wind does not blow from a specific direction), otherwise, it is not possible to get an estimation for a given field. Particularly under unstable conditions the flux footprint is smaller, and therefore there is a higher probability to observe a single crop (Figure 11b). Consequently, we combine multiple sources of information to synergistically inform the flux tower observations at the ecosystem scaleand to decompose the relative contribution of each of the land cover types inside the flux footprint. This combined framework can be used to study aspects about the heterogeneity of the landscape beyond what a tower could provide.

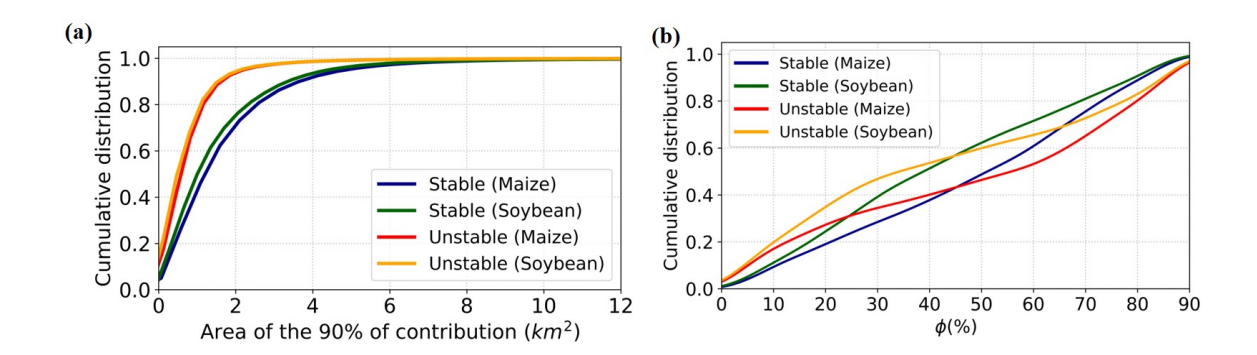


Figure 11. Cumulative seasonal behavior of the relative flux footprint contribution due to maize and soybean. The cumulative distribution of the (a) area of 90% of flux footprint contribution and the (b) flux footprint relative contribution, show the behavior of each crop type under stable (blue and green, for maize and soybean, respectively) and unstable (red and orange, for maize and soybean, respectively) atmospheric conditions.

# 4.5 Organized heterogeneity and hydroclimatological drivers explain high 2017 $CO_2$ uptake

As mentioned in Section 4.1, the annual net  $CO_2$  budget is driven by the combined action of (1) hydroclimatological drivers acting on the ecosystem and (2) the difference in the fraction of maize and soybean in the flux footprint due to the organized heterogeneity of the land cover. Here we use results from the relative contribution analysis to understand the relationship between the lowest crop yield and the largest net  $CO_2$  budget observed in 2017, in comparison to 2016 and 2018 (Table 2). The USDA provides crop yields at

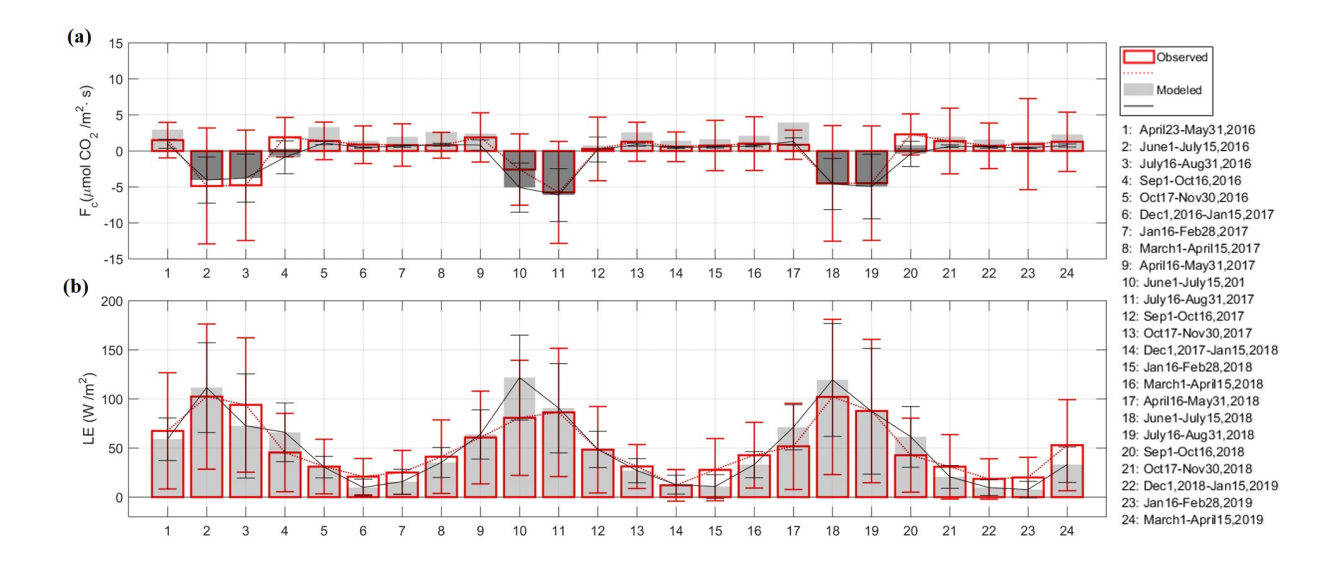


Figure 12. Difference between flux tower observations (red) and modeled (gray) daily averaged fluxes in 6-week windows (corresponding to Figure 6), for (a) carbon dioxide flux,  $F_c$ , and (b) latent heat flux,  $E_c$ . The error bars show the standard deviation of the daily average over the 6-week period for the observed (red) and modeled data (black). The segmented line in red shows the behavior of the daily averaged observations, while the continuous black line similarly shows the modeled data.

544

545

546

547

548

550

551

552

553

554

555

556

557

558

the county scale for Piatt county, Illinois (NASS, 2016-2018)(Figure 13a), which we assume is representative of yields at the study site. This low yield can be partially attributed to the high solar radiation and low rainfall during the 2017 growing season (Figure 5). Next we consider how the different contributions of maize and soybean inside the flux footprint can also inform this feature. From MLCan we obtain the net  $CO_2$  budget for each crop type during the growing seasons (Figure 13b). Assuming that the  $CO_2$  taken up is only used to produce dry matter (DM), and that the weight per bushel of DM for maize is 25.4 Kg/bushel and 27.2 Kg/bushel for soybean (Murphy, 1981), we estimate the net  $CO_2$  budget per unit yield for each crop type. Soybean has a larger  $CO_2$  uptake per unit yield than maize (Figure 13c). From the flux footprint analysis, the relative flux footprint contribution due to soybean is larger than from maize (Figure 13d). Using the previous results we estimate the net  $CO_2$  budget inside the flux footprint for each crop type and find that the highest  $CO_2$ uptake from soybean fields occurred in 2017 (Figure 13e). Given that soybean fields take up more  $CO_2$ , even in a drier, low-yield year we see more  $CO_2$  uptake for a year in which soybean is dominant inside the footprint. Also,  $CO_2$  release is muted from respiration by the drier conditions, further skewing the net flux towards high  $CO_2$  uptake (negative Fc).

Therefore, we observe that the higher annual net  $CO_2$  budget in the crop year 2017 is not only the effect of hydroclimatological conditions but to the particular contribution of soybean fields, which play a significant role in the higher uptake of  $CO_2$  observed that year. The combination of  $CO_2$  taken up by soybean fields and the lower respiration rate due to high temperatures and lower rainfall, influence the overall higher uptake of  $CO_2$  observed in 2017. These results show how the knowledge provided by multiple sources besides the observed  $F_c$  (i.e., MLCan and flux footprint modeling, as well as crop yield data), provides elements for an informed interpretation of the influence of the organized land cover heterogeneity on the behavior of observed land-atmosphere fluxes.

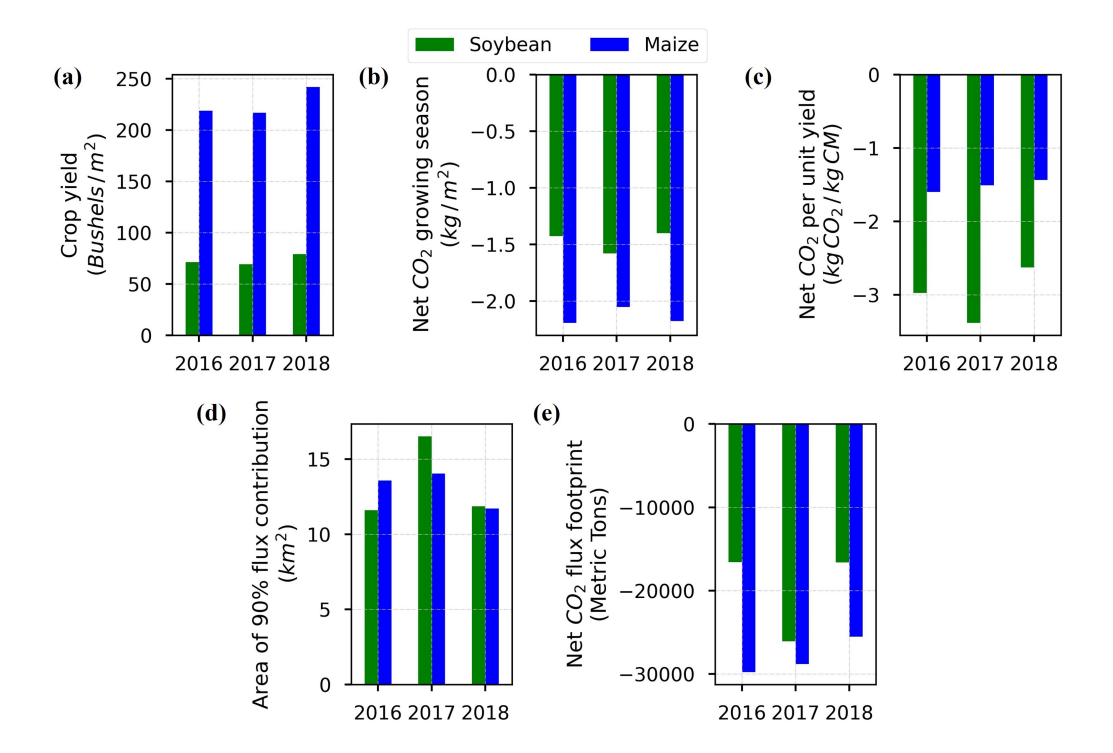


Figure 13. Relationship between crop yield and net  $CO_2$  during the growing season. (a) Crop yields at Piatt county are combined with (b) the net  $CO_2$  budget for each crop type during the growing seasons 2016-2018 estimated with MLCan, to calculate (c) the net  $CO_2$  uptake per unit yield of dry matter (DM) for soybean and maize. (d) The climatological flux footprint area for the 90% contribution is used to calculate (e) the net  $CO_2$  uptaked by maize and soybean fields at the study site during the growing season.

# 5 Summary and Conclusions

568

569

570

571

572

573

576

577

578

579

580

581

582

583

587

588

589

590

591

592

593

597

598

599

This study illustrates the important role of organized land cover heterogeneity on the observed land-atmosphere fluxes of heat, water, and  $CO_2$  that are measured at a tall tower. When the land cover is heterogeneous, inconsistencies in data interpretation can arise when only accounting for the vegetation type in the nearest field, or alternatively assuming that multiple crop types contribute equally to the observed flux. Area weighting based on the relative distribution of crop areas will not work as the fractional contribution from each crop changes with the dynamically changing flux footprint. Our framework combines flux footprint and ecohydrological modeling together with flux tower data to improve upon the understanding that could be obtained given any single information source.

Our approach of analyzing the flux contributions associated with the footprint of a tall tower footprint has some limitations, many of which could be improved upon in future studies. First, we consider that crops and soil components are the primary sources of  $CO_2$ , and that extremely low traffic in the nearby farm roads and other local sources are negligible contributors (the flux tower is strategically located away from major highways). However, it is difficult to establish how low automobile or mechanized farm equipment emissions may contribute to the observed  $CO_2$  fluxes, although we believe this will be very small. Second, the estimation of the flux footprint is not the only source of error, but tower observations and the ecohydrological model also have errors and as a result they contribute some uncertainty to our estimations. Third, we do not consider the variability in flux response across multiple fields cultivated with the same crop, but we assume a representative modeled flux. Specifically, we distinguish between "maize" or "soybean" patches and ignore other differentiating factors. In reality, all maize or soybean fields may not behave the same due to differences in cultivars, soil type, microtopographic variability, time of planting, etc. This assumption can be overcome through a distributed modeling approach if detailed data to support such modeling is available. For example, given a detailed map of soil texture or topography, the landscape could be divided into more than two components which could be modeled and attributed at higher resolution, e.g., "well-drained maize" or "drier soybean". This would enable testing of the assumption that vegetation type is the dominant differentiating factor between fluxes at different landscape patches. We anticipate that our study could be extended to study other natural and human-induced interventions on heterogeneous agricultural landscapes, such as varying wetness conditions,

601

602

603

604

605

606

607

608

610

611

612

613

614

615

616

617

618

619

620

621

622

623

624

625

626

627

628

629

630

LAI or planting dates, or for comparison with a remote sensing product. However, specifying spatially variable precipitation at these resolutions could remain a formidable challenge. This approach could also be applied to model evaluation, in that the representation of landscape heterogeneity should lead to an improved agreement between model results and observations, relative to the assumption that the tower measurements represent a single crop type or a homogeneous contribution from multiple crop types. In general, our method is relevant for the understanding of land-atmosphere fluxes in heterogeneous landscapes and can be extended towards the use of flux tower data as validation for models of these fluxes.

Our analyses show that the fluxes observed at the tall flux tower are the result of the combined action of (1) hydroclimatological drivers acting on the ecosystem, and (2) the difference in the fraction of maize and soybean in the flux footprint due to the organized heterogeneity of the land cover. In other words, the change in flux observed at every time of analysis at the tower (15 min) could either correlate to a change in flux from the crops or a shift in relative land cover contributions within the footprint, or both. For instance, we qualitatively demonstrated that the change in the relative contribution of fluxes due to two different land cover types can either increase or decrease the total flux observed at the tower. Therefore, we quantitatively showed that the spatial structure of the land cover, described here as "organized land cover heterogeneity" and characterized by the mosaic of crop fields, impacts the observed fluxes. Our focus on the relative contribution of maize and soybean fields inside the flux footprint shows the importance of an accurate description of the land cover and the use of an accurate flux footprint method. We recognize that it is equally important to accurately simulate the flux response of each vegetation species under the observed atmospheric drivers. All these are used to obtain the variability of the areal coverage and the temporal variability of the flux.

In an intensively managed agricultural landscape, where each land cover patch is easily identifiable by crop type (i.e. maize or soybean), we quantified the relative flux contribution of LE, H, and  $CO_2$ . At the study site, the cultivated fields where the flux contribution peaks are mainly due to one crop type, which explains the dominance in fluxes contribution given by maize-soybean-maize for 2016-2017-2018 crop years, respectively. This combined analysis makes it feasible to investigate questions regarding real and hypothetical land cover changes at an ecosystem scale and quantify the effects of different vegetation type on ecosystem fluxes.

# Acknowledgments

632

- This work was supported by NSF Grant EAR-1331906 for the Critical Zone Observatory
- for Intensively Managed Landscapes (IMLCZO), a multi-institutional collaborative effort,
- NSF grant OAC-1835834, and NSF Grant EAR-2012850 for the Critical Interface Network
- for Intensively Managed Landscapes (CINet). AEG is partially supported by NASA New
- Investigator Program Award 80NSSC21K0934. We thank Steve Sargent for supporting
- the data collection from the flux tower. The two-dimensional Flux Footprint Prediction
- 659 (FFP) model used in this study is available at https://footprint.kljun.net/ (Kljun et al.,
- 640 2015). MLCan2.0 model and data used in this research are publicly available at GitHub
- (https://github.com/HydroComplexity/ MLCan2.0/tree/master/Data/Goose\_Creek).
- DOI: 10.5281/zenodo.3931001 https:/zenodo.org/record/3931001).

# References

- Alekseychik, P., Korrensalo, A., Mammarella, I., Vesala, T., & Tuittila, E.-S. (2017). Re-
- lationship between aerodynamic roughness length and bulk sedge leaf area index in a
- mixed-species boreal mire complex. Geophysical Research Letters, 44 (11), 5836–5843.
- Anders, A. M., Bettis III, E. A., Grimley, D. A., Stumpf, A. J., & Kumar, P. (2018). Impacts
- of quaternary history on critical zone structure and processes: Examples and a con-
- ceptual model from the Intensively Managed Landscapes Critical Zone Observatory.
- Frontiers in Earth Science, 6, 24.
- Aubinet, M., Vesala, T., & Papale, D. (2012). Eddy covariance: A practical guide to

  measurement and data analysis. Springer Science & Business Media.
- 653 Biermann, T., Babel, W., Ma, W., Chen, X., Thiem, E., Ma, Y., & Foken, T. (2014).
- Turbulent flux observations and modelling over a shallow lake and a wet grassland
- in the nam co basin, tibetan plateau. Theoretical and applied climatology, 116(1),
- 656 301–316.
- Birch, H. (1958). The effect of soil drying on humus decomposition and nitrogen availability.
- Plant and soil, 10(1), 9–31.
- Burba, G. (2013). Eddy covariance method for scientific, industrial, agricultural and reg-
- ulatory applications: A field book on measuring ecosystem gas exchange and areal
- 661 emission rates. LI-Cor Biosciences.
- 662 Chi, J., Nilsson, M. B., Kljun, N., Wallerman, J., Fransson, J. E., Laudon, H., ... Peichl,
- M. (2019). The carbon balance of a managed boreal landscape measured from a tall

- tower in northern sweden. Agricultural and Forest Meteorology, 274, 29–41.
- Chi, J., Nilsson, M. B., Laudon, H., Lindroth, A., Wallerman, J., Fransson, J. E., ...
- Peichl, M. (2020). The net landscape carbon balance—integrating terrestrial and
- aquatic carbon fluxes in a managed boreal forest landscape in sweden. Global change
- biology, 26(4), 2353-2367.
- 669 Chu, H., Luo, X., Ouyang, Z., Chan, W. S., Dengel, S., Biraud, S. C., ... others (2021).
- Representativeness of eddy-covariance flux footprints for areas surrounding ameriflux
- sites. Agricultural and Forest Meteorology, 301, 108350.
- brewry, D., Kumar, P., Long, S., Bernacchi, C., Liang, X.-Z., & Sivapalan, M. (2010).
- Ecohydrological responses of dense canopies to environmental variability: 1. Inter-
- play between vertical structure and photosynthetic pathway. Journal of Geophysical
- Research: Biogeosciences, 115(G4).
- ECMWF. (2018). Era5 hourly data on single levels from 1979 to present. fifth gener-
- ation of ecmwf atmospheric reanalyses of the global climate. Retrieved 2021-01-04,
- from https://cds.climate.copernicus.eu/cdsapp#!/dataset/reanalysis-era5
- -single-levels?tab=form
- Foken, T. (2006). 50 years of the monin-obukhov similarity theory. Boundary-Layer
- Meteorology, 119(3), 431-447.
- Foufoula-Georgiou, E., Takbiri, Z., Czuba, J. A., & Schwenk, J. (2015). The change of
- nature and the nature of change in agricultural landscapes: Hydrologic regime shifts
- modulate ecological transitions. Water Resources Research, 51(8), 6649–6671.
- Gao, S., Niu, Z., Huang, N., & Hou, X. (2013). Estimating the leaf area index, height and
- biomass of maize using hj-1 and radarsat-2. International Journal of Applied Earth
- Observation and Geoinformation, 24, 1-8.
- Horst, T., & Weil, J. (1992). Footprint estimation for scalar flux measurements in the
- atmospheric surface layer. Boundary-Layer Meteorology, 59(3), 279–296.
- Jacobs, A. F., & Van Boxel, J. H. (1988). Changes of the displacement height and roughness
- length of maize during a growing season. Agricultural and Forest Meteorology, 42(1),
- 692 53<del>-</del>62.
- Kirby, S., Dobosy, R., Williamson, D., & Dumas, E. (2008). An aircraft-based data analysis
- method for discerning individual fluxes in a heterogeneous agricultural landscape.
- agricultural and forest meteorology, 148(3), 481–489.
- Kljun, N., Calanca, P., Rotach, M., & Schmid, H. P. (2015). A simple two-dimensional

- parameterisation for flux footprint prediction (ffp). Geoscientific Model Development,
  8(11), 3695–3713.
- Kumar, P., Le, P. V., Papanicolaou, A. T., Rhoads, B. L., Anders, A. M., Stumpf, A.,
- ... Belmont, P. (2018). Critical transition in critical zone of Intensively Managed
   Landscapes. Anthropocene, 22, 10–19.
- Le, P. V., & Kumar, P. (2014). Power law scaling of topographic depressions and their hydrologic connectivity. Geophysical Research Letters, 41(5), 1553–1559.
- Le, P. V., Kumar, P., Drewry, D. T., & Quijano, J. C. (2012). A graphical user interface for numerical modeling of acclimation responses of vegetation to climate change.
- Computers & Geosciences, 49, 91–101.
- Leclerc, M. Y., & Foken, T. (2014). Footprints in micrometeorology and ecology (Vol. 239).

  Springer.
- Lee, T. R., & De Wekker, S. F. (2016). Estimating daytime planetary boundary layer heights
  over a valley from rawinsonde observations at a nearby airport: an application to the
  page valley in virginia, united states. Journal of Applied Meteorology and Climatology,
  55(3), 791–809.
- Lei, N., & Han, J. (2020). Effect of precipitation on respiration of different reconstructed soils. *Scientific reports*, 10(1), 1–10.
- Licor. (2021). Tovi. Retrieved 2021-08-13, from https://licor.com/tovi/
- Masson-Delmotte, V., P., Z., A., P., S. L., C., C., P., S., B., ... B., Z. (2021). Ipcc, 2021:

  Climate change 2021: The physical science basis. contribution of working group i to the

  sixth assessment report of the intergovernmental panel on climate change. Cambridge
  University Press.
- Mishra, V., & Cherkauer, K. A. (2010). Retrospective droughts in the crop growing season:

  Implications to corn and soybean yield in the Midwestern United States. Agricultural
  and Forest Meteorology, 150 (7-8), 1030–1045.
- Monfreda, C., Ramankutty, N., & Foley, J. A. (2008). Farming the planet: 2. Geographic distribution of crop areas, yields, physiological types, and net primary production in the year 2000. Global biogeochemical cycles, 22(1).
- Murphy, W. J. (1981). Tables for weights and measurements-crops.
- Myneni, R., Knyazikhin, Y., & Park, T. (2015). Mod15a2h modis/terra leaf area index/fpar 8-day 14 global 500 m sin grid v006. NASA EOSDIS Land Processes DAAC.
- NASS, U. (2010). Field crops: Usual planting and harvesting dates. USDA National

- Agricultural Statistics Service, Agricultural Handbook, 628.
- NASS, U. (2016-2018). Illinois corn and soybean county estimates.
- Nemani, R., White, M., Thornton, P., Nishida, K., Reddy, S., Jenkins, J., & Running, S.
- 733 (2002). Recent trends in hydrologic balance have enhanced the terrestrial carbon sink
- in the United States. Geophysical Research Letters, 29(10), 106–1.
- Nguy-Robertson, A., Gitelson, A., Peng, Y., Viña, A., Arkebauer, T., & Rundquist, D.
- 736 (2012). Green leaf area index estimation in maize and soybean: Combining vegetation
- indices to achieve maximal sensitivity. Agronomy Journal, 104(5), 1336–1347.
- Pasquill, F., & Smith, F. (1983). Atmospheric diffusion, third ed. Wiley, New York.
- Richardson, M., & Kumar, P. (2017). Critical zone services as environmental assessment
- criteria in Intensively Managed Landscapes. Earth's Future, 5(6), 617–632.
- Schmid, H. (1994). Source areas for scalars and scalar fluxes. Boundary-Layer Meteorology,
- 67(3), 293-318.
- Schuepp, P., Leclerc, M., MacPherson, J., & Desjardins, R. (1990). Footprint prediction
- of scalar fluxes from analytical solutions of the diffusion equation. Boundary-Layer
- 745 Meteorology, 50 (1-4), 355-373.
- Seidel, D. J., Zhang, Y., Beljaars, A., Golaz, J.-C., Jacobson, A. R., & Medeiros, B. (2012).
- Climatology of the planetary boundary layer over the continental united states and
- europe. Journal of Geophysical Research: Atmospheres, 117(D17).
- Stull, R. B. (2012). An introduction to boundary layer meteorology (Vol. 13). Springer
- Science & Business Media.
- Tuovinen, J.-P., Aurela, M., Hatakka, J., Räsänen, A., Virtanen, T., Mikola, J., ... Lau-
- rila, T. (2019). Interpreting eddy covariance data from heterogeneous siberian tun-
- dra: land-cover-specific methane fluxes and spatial representativeness. *Biogeosciences*,
- 16(2), 255-274.
- Vesala, T., Kljun, N., Rannik, Ü., Rinne, J., Sogachev, A., Markkanen, T., ... Leclerc, M.
- 756 (2008). Flux and concentration footprint modelling: State of the art. Environmental
- Pollution, 152(3), 653-666.
- Vogelezang, D., & Holtslag, A. A. (1996). Evaluation and model impacts of alternative
- boundary-layer height formulations. Boundary-Layer Meteorology, 81(3), 245–269.
- Warner, R. E., Havera, S. P., David, L. M., & Siemers, R. J. (1989). Seasonal abundance of
- vaste corn and soybeans in Illinois. The Journal of wildlife management, 142–148.
- Wilson, C. G., Abban, B., Keefer, L. L., Wacha, K., Dermisis, D., Giannopoulos, C., ...

Papanicolaou, A. (2018). The Intensively Managed Landscape Critical Zone Observa-763 tory: A scientific testbed for understanding critical zone processes in agroecosystems. 764 Vadose Zone Journal, 17(1). 765 Yan, Q., Le, P. V., Woo, D. K., Hou, T., Filley, T., & Kumar, P. (2019). Three-dimensional 766 modeling of the coevolution of landscape and soil organic carbon. Water Resources 767 Research, 55(2), 1218-1241.768 Zhang, H., & Wen, X. (2015). Flux footprint climatology estimated by three analytical 769 models over a subtropical coniferous plantation in southeast china. Journal of Mete-770  $orological\ Research,\ 29(4),\ 654-666.$